Hindawi Publishing Corporation
Discrete Dynamics in Nature and Society
Volume 2012, Article ID 631476, 15 pages
doi:10.1155/2012/631476

Research Article

Chaos and Control in Coronary Artery System

Yanxiang Shi

School of Mathematical Sciences, Shanxi University, Taiyuan 030006, China

Correspondence should be addressed to Yanxiang Shi, hongyu@sxu.edu.cn

Received 5 April 2011; Accepted 9 November 2011

Academic Editor: Vladimir Gontar

Two types of coronary artery system N-type and S-type, are investigated. The threshold conditions for the occurrence of Smale horseshoe chaos are obtained by using Melnikov method. Numerical simulations including phase portraits, potential diagram, homoclinic bifurcation curve diagrams, bifurcation diagrams, and Poincaré maps not only prove the correctness of theoretical analysis but also show the interesting bifurcation diagrams and the more new complex dynamical behaviors. Numerical simulations are used to investigate the nonlinear dynamical characteristics and complexity of the two systems, revealing bifurcation forms and the road leading to chaotic motion. Finally the chaotic states of the two systems are effectively controlled by two control methods: variable feedback control and coupled feedback control.

1. Introduction

Chaotic science is one of the three major scientific achievements in 20th century. Since the Lorenz system was discovered in 1963, many new chaotic systems have been successively raised [1–4]. The proposal of these systems promotes the theory research of chaos to continue indepth and provides supports for the application of chaos in the field of engineering technology, for example, information processes, secure communication. There are many in-depth conclusions on the chaotic motion under the periodic or quasiperiodic perturbation. Jing and Wang [5], and Jing et al. [6, 7] showed the complex dynamics in Duffing system, including bifurcation and chaos.

The coronary artery system driven by periodic excitations is a typical nonlinear vibration system and has a rich dynamic behavior. According to pathological studies, the heart coronary artery atherosclerosis and coronary artery spasm are the cause of myocardial infarction. From the mathematical point of view, the vascular spasm is the chaotic state of vasomotor. There are two kinds of blood vessels: N-type and S-type.

(A) N-Type Model

For N-type model, if $z(t)$ is pressure difference and $x(t)$ is diameter change, then the nonlinear mathematical model [8] of the blood vessels can be written as

$$\begin{aligned} \frac{dz}{dt} &= \lambda\left[-x + x^3 - z\right] + \lambda\frac{dx}{dt}, \\ \frac{dx}{dt} &= -bz - cx. \end{aligned} \tag{1.1}$$

The type can be rewritten as

$$\frac{d^2x}{dt^2} = (b\lambda - \lambda c)x - b\lambda x^3 - (\lambda + b\lambda + c)\frac{dx}{dt}. \tag{1.2}$$

Let $b\lambda - \lambda c > 0$, $\lambda + b\lambda + c = \varepsilon\delta$, $b\lambda - \lambda c = A + \varepsilon r_1$, $b\lambda = B + \varepsilon r_2$, and $dx/dt = y$, by adding periodic interference $\varepsilon r \cos\omega t$, then the above equation can be rewritten as

$$\begin{aligned} \dot{x} &= y, \\ \dot{y} &= Ax - Bx^3 - \varepsilon\delta y + \varepsilon r\cos\omega t + \varepsilon r_1 x - \varepsilon r_2 x^3. \end{aligned} \tag{1.3}$$

(B) S-Type Model

For S-type model, the nonlinear mathematical model [8] can be written as

$$\begin{aligned} \frac{dz}{dt} &= \lambda\left(x + z - z^3 + \frac{dx}{dt}\right), \\ \frac{dx}{dt} &= -az - bx. \end{aligned} \tag{1.4}$$

The type can be rewritten as

$$\frac{d^2x}{dt^2} = x(\lambda b - \lambda a) + \frac{dx}{dt}(\lambda - a\lambda - b) - \frac{\lambda}{a^2}b^3x^3 - \frac{\lambda}{a^2}\left(\frac{dx}{dt}\right)^3 - \frac{\lambda}{a^2}3bx\left(\frac{dx}{dt}\right)^2 - \frac{3\lambda b^2}{a^2}x^2\frac{dx}{dt}. \tag{1.5}$$

Let $\lambda - a\lambda - b = -\varepsilon\delta$, $\lambda/a^2 = \varepsilon\delta_1$, $(\lambda/a^2)3b = \varepsilon\delta_2$, $3\lambda b^2/a^2 = \varepsilon\delta_3$, $\lambda b - \lambda a = F + \varepsilon r_1$, $(\lambda/a^2)b^3 = D + \varepsilon r_2$ and $dx/dt = y$, by adding interference $\varepsilon r\cos\omega t$, then the above equation can be rewritten as

$$\begin{aligned} \dot{x} &= y, \\ \dot{y} &= Fx - Dx^3 - \varepsilon\delta y - \varepsilon\delta_1 y^3 - \varepsilon\delta_2 y^2 x - \varepsilon\delta_3 x^2 y + \varepsilon r\cos\omega t + \varepsilon r_1 x - \varepsilon r_2 x^3. \end{aligned} \tag{1.6}$$

The model of coronary artery system and its chaotic motion were given in [9], and by using Melnikov method the conditions for chaos of the two types are shown.

Melnikov method is an important theoretical way to determine whether there is chaos in two-dimensional system [10–12]. However, there has been less attention to chaos control of the coronary artery system in all kinds of literatures, as a major topic of control science, it is necessary to investigate in detail.

In this paper, the system (1.3) and (1.6) are analyzed from two aspects: quality and quantity. By Melnikov method the thresholds of Smale horseshoe chaos for the system (1.3) and (1.6) are given. By numerical simulations, including phase portraits, potential diagram, homoclinic bifurcation curve diagrams, bifurcation diagrams, and Pioncaré maps, the dynamical characteristics of the system (1.3) and (1.6) with the changes of the bifurcation parameters are reflected intuitively, and it is proved that the system (1.3) and (1.6) exists chaos indeed. Finally, the chaos of the system (1.3) and (1.6) is controlled to stable periodic orbits by two kinds of control methods.

The paper is organized as follows. In Section 2, we briefly describe the necessary conditions of existence of chaos resulting from the homoclinic bifurcation of two systems. The numerical simulations which give support to the theoretical analysis are performed in Section 3. The chaos in Section 3 is controlled by two kinds of chaos control methods in Section 4: variable feedback control and coupled feedback control. Finally, we make conclusions in Section 5.

2. The Necessary Conditions for Chaos

If $\varepsilon = 0$, the system (1.3) is considered as an Hamilton system with Hamilton function

$$H(x,y) = \frac{1}{2}y^2 - \frac{A}{2}x^2 + \frac{B}{4}x^4, \tag{2.1}$$

and the function

$$V(x) = -\frac{A}{2}x^2 + \frac{B}{4}x^4 \tag{2.2}$$

is called the potential function. There are three fixed points as $\varepsilon = 0 : (0,0)$, $(\pm\sqrt{A/B},0)$, where $(0,0)$ is saddle, and $(\pm\sqrt{A/B},0)$ are centers. There are two homoclinic orbits $\Gamma_N^{\pm}$:

$$\begin{aligned} x_0(t) &= \pm\sqrt{\frac{2A}{B}}\operatorname{sech}\sqrt{A}t, \\ y_0(t) &= \mp\sqrt{\frac{2}{B}}A\operatorname{sech}\sqrt{A}t\tanh\sqrt{A}t. \end{aligned} \tag{2.3}$$

The phase portrait and potential diagram of the system (1.3) as $\varepsilon = 0$ are shown in Figures 1(a) and 1(b), respectively, where $A = B = 1$. In Figure 1(a) the saddle $(0,0)$ is connected itself by two homoclinic orbits $\Gamma_N^{\pm}$.

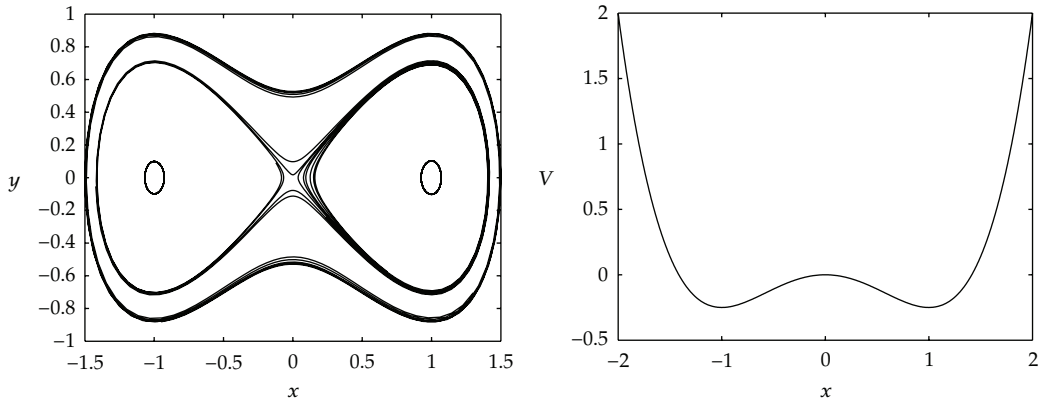

Figure 1: Phase portrait and potential of the system (1.3) and (1.6) as $\varepsilon = 0$. System (1.3): $A = B = 1$; System (1.6): $F = D = 1$.

The Melnikov function for homoclinic orbits $\Gamma_N^{\pm}$ can be given by

$$M(t_0) = \int_{-\infty}^{+\infty} y_0(t)\left[r\cos\omega(t-t_0) - \delta y_0(t)\right]dt + \int_{-\infty}^{+\infty} y_0(t)\left[r_1 x_0(t) - r_2 x_0^3(t)\right]dt. \tag{2.4}$$

According to the expression of homoclinic orbits $\Gamma_N^{\pm}$ in (2.3), the Melnikov function can be simplified as

$$M(t_0) = \frac{-A\sqrt{2}r}{\sqrt{B}\sqrt{A}}\pi\omega\frac{1}{\sqrt{A}}\operatorname{sech}\frac{\pi\omega}{2\sqrt{A}}\sin\omega\sqrt{A}t_0 - \frac{4}{3}\delta\frac{A^2}{B}\frac{1}{\sqrt{A}}. \tag{2.5}$$

Thus, if

$$\frac{r}{\delta} > \frac{(4/3)A^{3/2}}{\sqrt{2}\sqrt{B}\pi\omega\operatorname{sech}\left(\pi\omega/2\sqrt{A}\right)}, \tag{2.6}$$

then $M(t_0)$ has a simple zero and Smale chaos exists in the system (1.3).

If $\varepsilon = 0$, the system (1.6) is Hamilton system with Hamilton function

$$H(x,y) = \frac{1}{2}y^2 - \frac{F}{2}x^2 + \frac{D}{4}x^4, \tag{2.7}$$

and the potential function is

$$V(x) = -\frac{F}{2}x^2 + \frac{D}{4}x^4. \tag{2.8}$$

There are three fixed points in system (1.6) as $\varepsilon = 0 : (0,0), (\pm\sqrt{F/D}, 0)$, where $(0,0)$ is saddle, and $(\pm\sqrt{F/D}, 0)$ are centers. There are two homoclinic orbits $\Gamma_S^{\pm}$:

$$x_0(t) = \pm\sqrt{\frac{2F}{D}}\operatorname{sech}\sqrt{F}t,$$
$$y_0(t) = \mp\sqrt{\frac{2}{D}}F\operatorname{sech}\sqrt{F}t\tanh\sqrt{F}t. \tag{2.9}$$

The phase portrait and potential diagram of the system (1.6) as $\varepsilon = 0$ are shown in Figures 1(a) and 1(b), respectively, where $F = D = 1$. In Figure 1(a) the saddle $(0,0)$ is connected itself by two homoclinic orbits $\Gamma_S^{\pm}$.

The Melnikov function for homoclinic orbits $\Gamma_S^{\pm}$ can be given by

$$\begin{aligned} &M(t_0) \\ &= \int_{-\infty}^{+\infty} y_0(t)\left[r\cos\omega(t-t_0) - \delta y_0(t) - \delta_1 y_0^3(t) - \delta_2 y_0^2(t)x_0(t) - \delta_3 y_0(t)x_0^2(t) - r_1 x_0(t) - r_2 x_0^3(t)\right]dt \\ &= rI_1 - \delta I_2 - \delta_1 I_3 - \delta_2 I_4 - \delta_3 I_5 - r_1 I_6 - r_2 I_7, \end{aligned} \tag{2.10}$$

where

$$I_1 = \frac{\sqrt{2}}{\sqrt{D}}\pi\omega\operatorname{sech}\frac{\pi\omega}{2\sqrt{F}}\sin\omega\sqrt{F}t_0, \qquad I_2 = -\frac{F^{3/2}}{D}\frac{4}{3}, \qquad I_3 = \frac{4F^{3/2}}{D^2}\left(-\frac{316}{35}\right),$$
$$I_4 = I_6 = I_7 = 0, \qquad I_5 = \frac{4}{15}\frac{4F^3}{D^2}\frac{1}{\sqrt{F}}. \tag{2.11}$$

If

$$\left|\frac{\delta\left(4F^{3/2}/3D\right) + \delta_1\left(4F^{3/2}/D^2\right)(-316/35) + \delta_3\left(4F^3/D^2\right)\left(1/\sqrt{F}\right)(4/15)}{r\left(\sqrt{2}/\sqrt{D}\right)\pi\omega\operatorname{sech}\left(\pi\omega/2\sqrt{F}\right)}\right| \leqslant 1, \tag{2.12}$$

then $M(t_0)$ has a simple zero and Smale chaos exists in the system (1.6).

3. The Numerical Simulations

The purpose of this section is to provide a basis for the preceding theoretical analysis by using numerical simulation, and to seek more complex dynamical behaviors of the two systems.

First, numerical simulations are performed for the system (1.3).

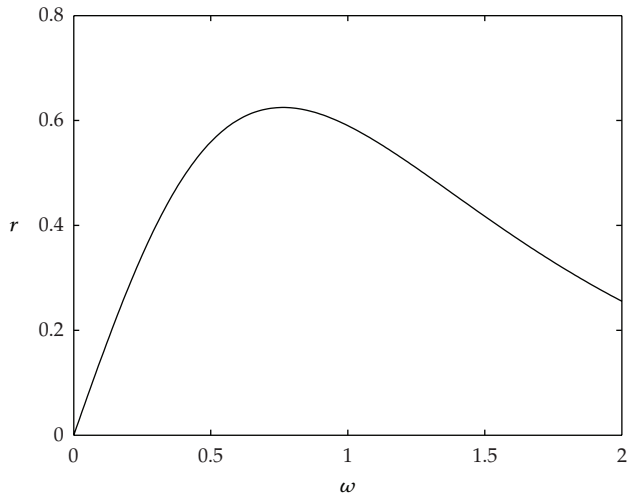

Figure 2: Homoclinic bifurcation curve for Smale horseshoe chaos in the (ω, r) plane for $\delta = 0.5$, $A = 1$, and $B = 1$. Above the curve transverse intersections of homoclinic orbits occur.

The homoclinic bifurcation curve for Smale chaos is in the (ω, r) plane for $\delta = 0.5$, $A = 1$, and $B = 1$ in Figure 2. In the parameter region below the bifurcation curve and no transverse intersection of stable and unstable manifolds of saddle occurs and above the bifurcation curve the transverse intersections of stable and unstable manifolds of the saddle occur. Just above the homoclinic bifurcation curve, onset of cross-well chaos is expected.

In order to show what happens to the solutions and attractors as one crosses the homoclinic bifurcation curve, we plot the bifurcation diagram of the system (1.3) in (r, x) plane for $A = 1$, $B = 1$, $\delta = 0.5$, $\omega = 1$, $r_1 = 0.01$, and $r_2 = 0.001$ in Figure 3(a). From it, we can see the period-doubling bifurcation from period-1 orbit to chaos, intermittent dynamics at $r \approx 0.825$, and chaotic region with periodic windows. For clarity, the local amplified bifurcation diagrams of Figure 3(a) for $0.30 \leqslant r \leqslant 0.50$ (amplified period-double section), $0.40 \leqslant r \leqslant 0.65$ (amplified chaotic window), and $0.55 \leqslant r \leqslant 0.80$ (amplified chaotic window) are given in Figures 3(b)–3(d). As r increases from $r = 0$, the system (1.3) is in stable state of period-1 orbit, and, at $r = 0.34669$, period-doubling bifurcation occurs; that is, the original period-1 orbit becomes unstable, and stable period-2 orbit is produced. With the r increasing, the deeper period-doubling bifurcation occurs and generates stable period-4 orbit, period-8 orbit, and period-16 orbit,.... It shows that the onset of chaos is at $r = 0.58717$. Analytically predicted Melnikov threshold value is $r = 0.5902$. The two values are almost similar, and it is indicated that the theoretical analysis is consistent to the numerical simulation. From Figure 3(c) we can find period-5 window, and period-3 window. The existence of a period-3 window is demonstrated in Figure 3(d). Chaos disappears at $r = 0.82966$, and the system (1.3) eventually becomes stable period-1 orbit. The phase portraits of the system (1.3) for $r = 0.1$ (period-1 orbit), $r = 0.355$ (period-4 orbit), $r = 0.8$ (chaos), and $r = 0.9$ (period-1 orbit) are plotted in Figures 4(a)–4(d). The Pioncaré maps for $r = 0.2$, $r = 0.355$, $r = 0.8$, and $r = 0.9$ are shown in Figures 4(e)–4(h). We can see the process from the periodic orbits to chaos, and then from chaos to periodic orbits.

Next, numerical simulations are performed for the system (1.6).

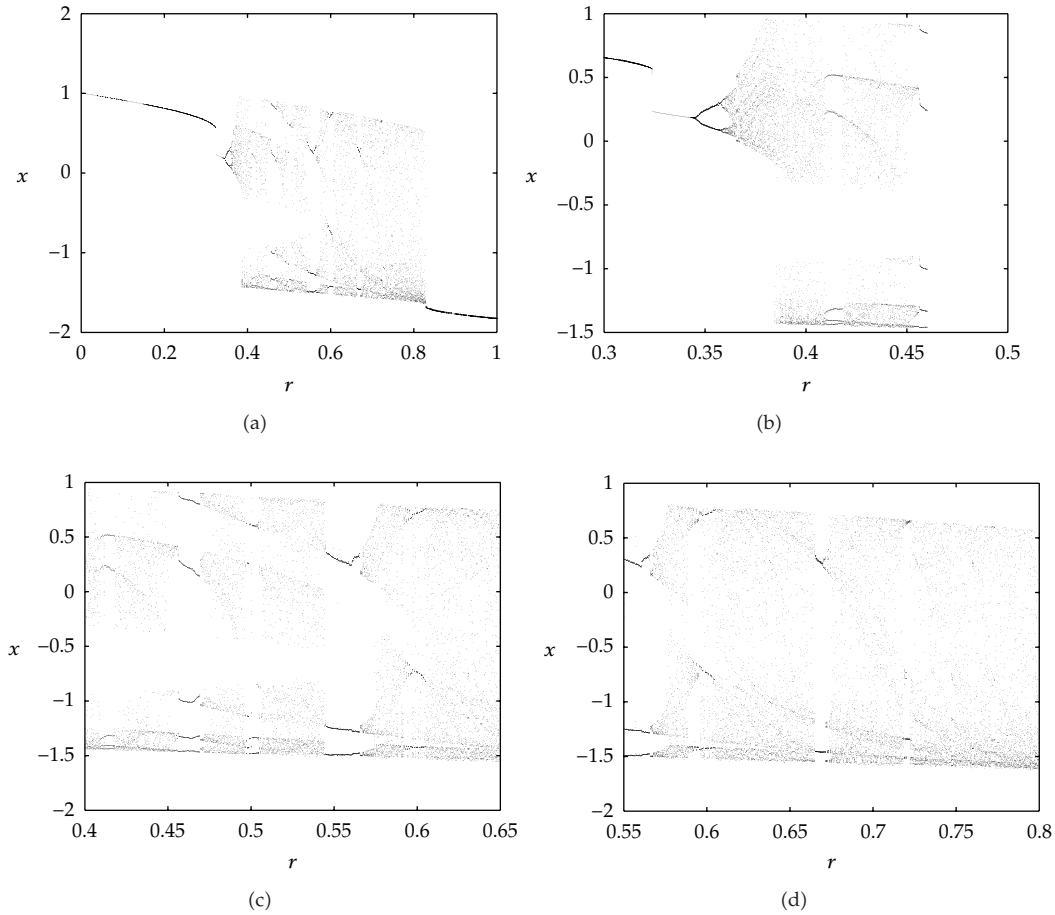

Figure 3: (a) Bifurcation diagram of the system (1.3) in (r, x) plane for $A = 1$, $B = 1$, $\delta = 0.5$, $\omega = 1$, $r_1 = 0.01$, and $r_2 = 0.001$. (b, c, and d) Amplified bifurcation diagram of Figure 3(a): (b) $0.30 \leqslant r \leqslant 0.50$; (c) $0.40 \leqslant r \leqslant 0.65$; (d) $0.55 \leqslant r \leqslant 0.80$.

The homoclinic bifurcation curve for Smale chaos in the (ω, r) plane for $\delta = 0.5$, $F = 1$, $D = 1$, $\delta_1 = 0.05$, and $\delta_3 = 0.2$ in Figure 5. In the parameter region below the bifurcation curve, no transverse intersection of stable and unstable manifolds of saddle occurs, and above the bifurcation curve the transverse intersections of stable and unstable manifolds of the saddle occur. Just above the homoclinic bifurcation curve, onset of cross-well chaos is expected.

We plot the bifurcation diagram of the system (1.6) in $r \in (0.4, 1.2)$ for $F = 1, D = 1, \delta = 0.5$, $\delta_1 = 0.05$, $\delta_2 = 0.1$, $\delta_3 = 0.2$, $\omega = 1$, $r_1 = 0.01$, and $r_2 = 0.001$ in Figure 6(a). From it, we can see the period-doubling bifurcations from period-1 orbit leading to chaos, intermittent dynamics at $r \approx 1.148$, chaos with period windows. The local amplified bifurcation diagrams of Figure 6(a) for $r \in (0.55, 0.80)$, $r \in (0.78, 0.88)$ and $r \in (0.80, 1.20)$ are given in Figures 6(b)–6(d). It can be seen the existence of period-doubling bifurcations, and different period windows: (b) period-3; (c) period-2; (d) periodic-3,4,5. The phase portraits of the system (1.6) for $r = 0.68$ (period-3 orbit), $r = 0.91$ (period-5 orbit), $r = 0.97$ (period-3 orbit) and $r = 1.1$

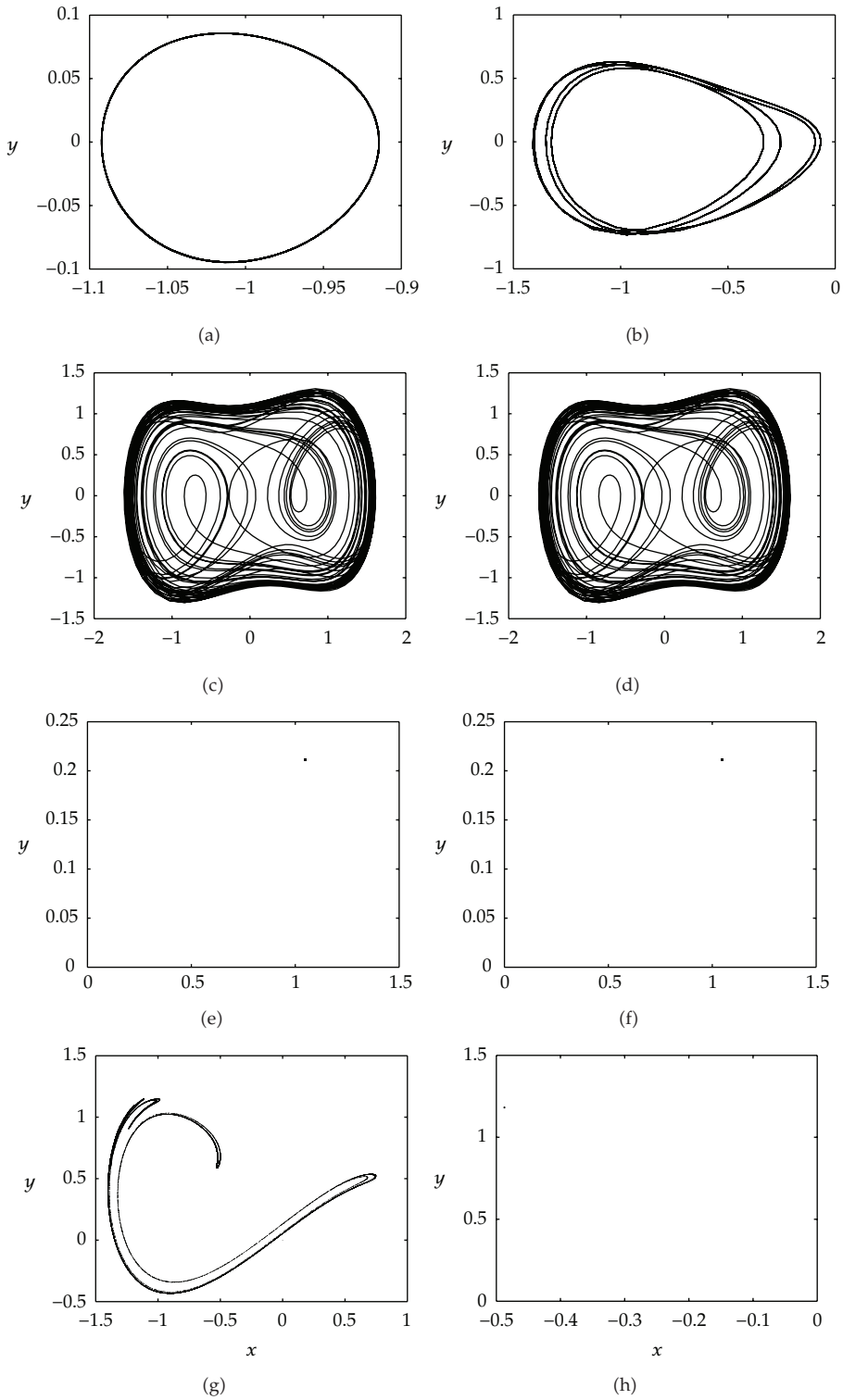

Figure 4: (a, b, c, and d) Phase portraits of the system (1.3); (e, f, g, and h) Pioncaré maps of the system (1.3).

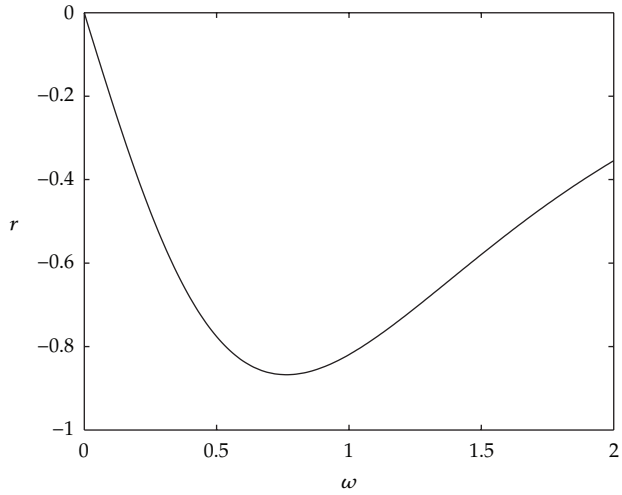

Figure 5: Homoclinic bifurcation curve for Smale horseshoe chaos in the (ω, r) plane for $\delta = 0.5$, $F = 1$, $D = 1$, $\delta_1 = 0.05$, and $\delta_3 = 0.2$. Above the curve transverse intersections of homoclinic orbits occur.

(chaos) are plotted in Figures 7(a)–7(d). The Pioncaré maps corresponding to Figures 7(a)–7(d) are shown in Figures 7(e)–7(h).

4. Chaos Control

The above-numerical results show that the systems is in chaotic state for some parameters. In order to suppress and eliminate the chaotic behaviors, it is necessary to control the chaotic motions. Two methods of control are proposed in this section. The results are demonstrated by numerical results, that is, bifurcation diagram and phase portrait.

4.1. Variable Feedback Control

By using variable feedback control, the chaos of the system (1.3) is controlled. The dynamic behavior of original system persists due to the change of small parameter having no effect on the system. This method not only can stabilize the unstable periodic orbit in the original system, but also can create a new cycle of orbits.

By adding a feedback variable K (K is the adjustable feedback factor) to the first equation, the system (1.3) can be rewritten as

$$\begin{aligned} \dot{x} &= y - Kx, \\ \dot{y} &= Ax - Bx^3 - \varepsilon\delta y + \varepsilon r \cos\omega t + \varepsilon r_1 x - \varepsilon r_2 x^3. \end{aligned} \tag{4.1}$$

Even if the feedback coefficient is small, it can also significantly weaken the chaotic behavior, so the chaotic behavior of the system (1.3) can be inhibited by selecting the appropriate K in bifurcation diagram. The bifurcation diagram of the system (4.1) at $K \in (0, 1)$ for $A = 1$, $B = 1$, $\delta = 0.5$, $\omega = 1$, $r_1 = 0.01$, $r_2 = 0.001$, $r = 0.8$ is shown in Figure 8(a).

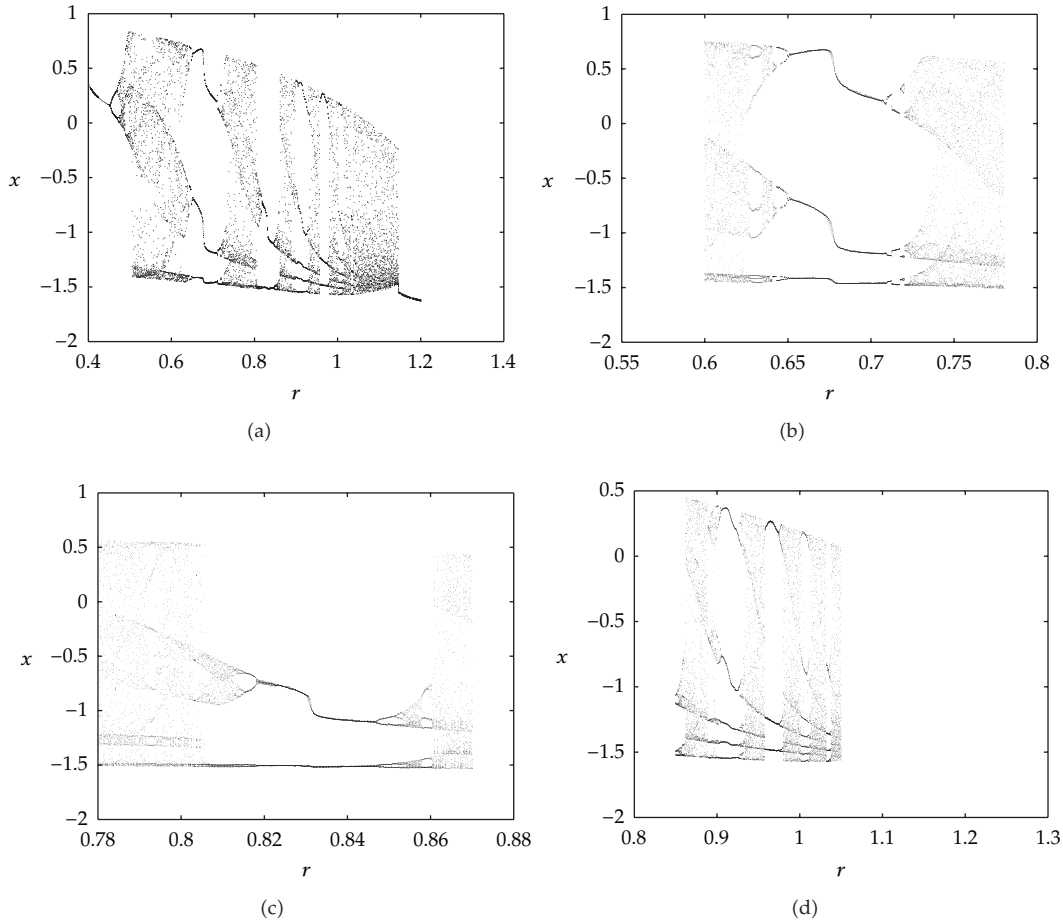

Figure 6: (a) Bifurcation diagram of the system (1.6) in (r, x) plane for $F = 1$, $D = 1$, $\delta = 0.5$, $\delta_1 = 0.05$, $\delta_2 = 0.1$, $\delta_3 = 0.2$, $\omega = 1$, $r_1 = 0.01$, and $r_2 = 0.001$. (b, c, and d) Amplified bifurcation diagram of Figure 6(a): (b) $0.55 \leqslant r \leqslant 0.80$; (c) $0.78 \leqslant r \leqslant 0.88$; (d) $0.80 \leqslant r \leqslant 1.20$.

From this, we can see the chaos region with period-2,3 windows. Near $K = 0.59319$, system occurs inverse period-double bifurcation, that is, chaos disappears,. . ., period-16 orbit, period-8 orbit, period-4 orbit, period-2 orbit, until the stable period-1 orbit are produced. It shows that the feedback variable K has impact of suppression on the chaos of the original system, chaos disappears and the periodic orbits produce. For clarity, the phase portraits of the system (4.1) for $K = 0.05$ (chaos), $K = 0.4$ (period-3 orbit), and $K = 0.8$ (period-1 orbit) are plotted in Figures 8(b)-8(d). The Pioncaré maps for $K = 0.4$ and $K = 0.8$ are shown in Figures 8(e) and 8(f).

By numerical simulation (Bifurcation diagrams, different phase portraits, and Pioncaré maps of the system (4.1) under feedback variable K ($K > 0$)), chaos, generated in Section 3, is controlled. Through numerical simulation, it is found that variable feedback control method has good control effect, and the method is simple and easy to implement, without too much of the knowledge of the controlled system, and it controls chaos stably and reliably.

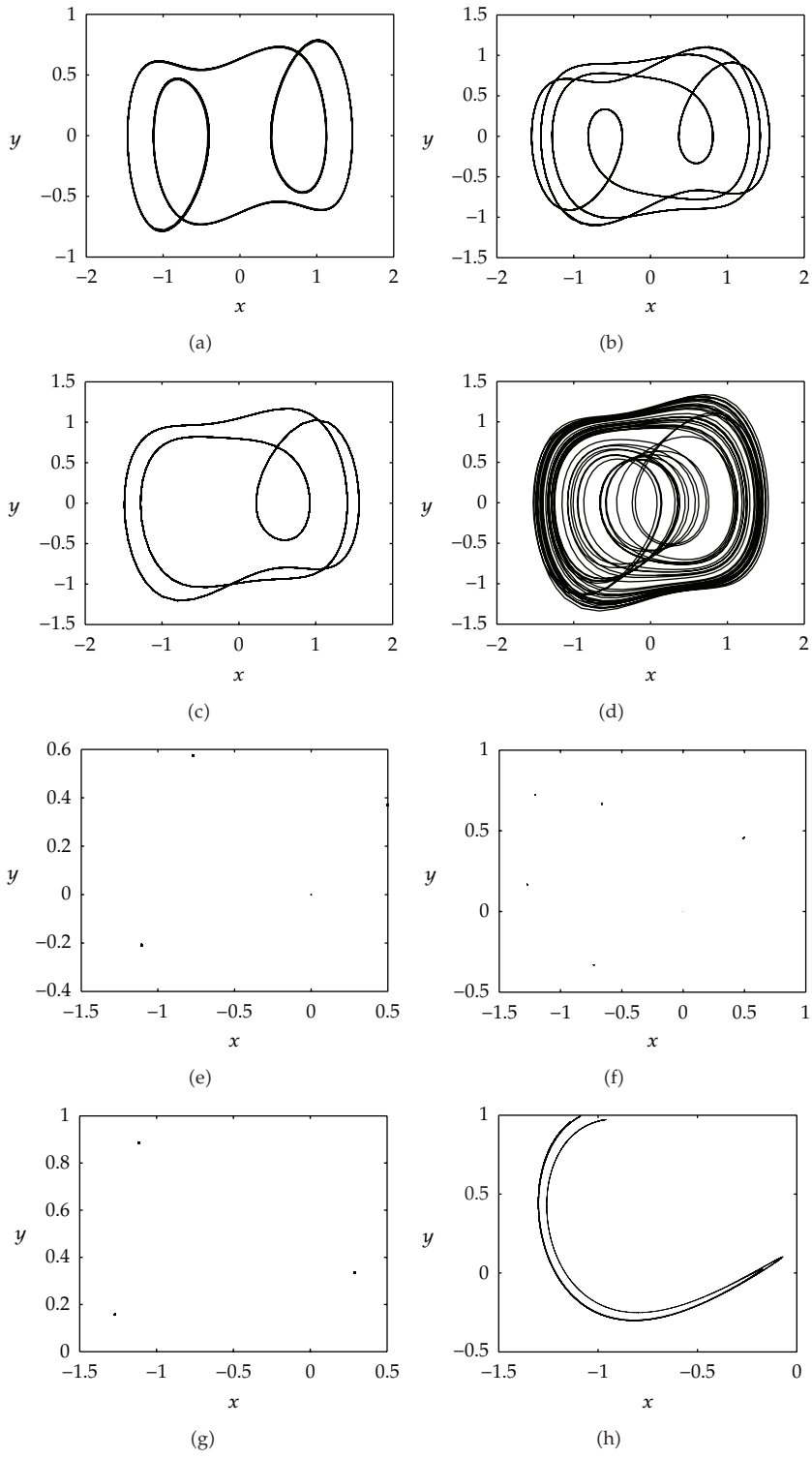

Figure 7: (a,b,c, and d) Phase portraits of the system (1.6); (e, f, g, and h) Pioncaré maps of the system (1.6).

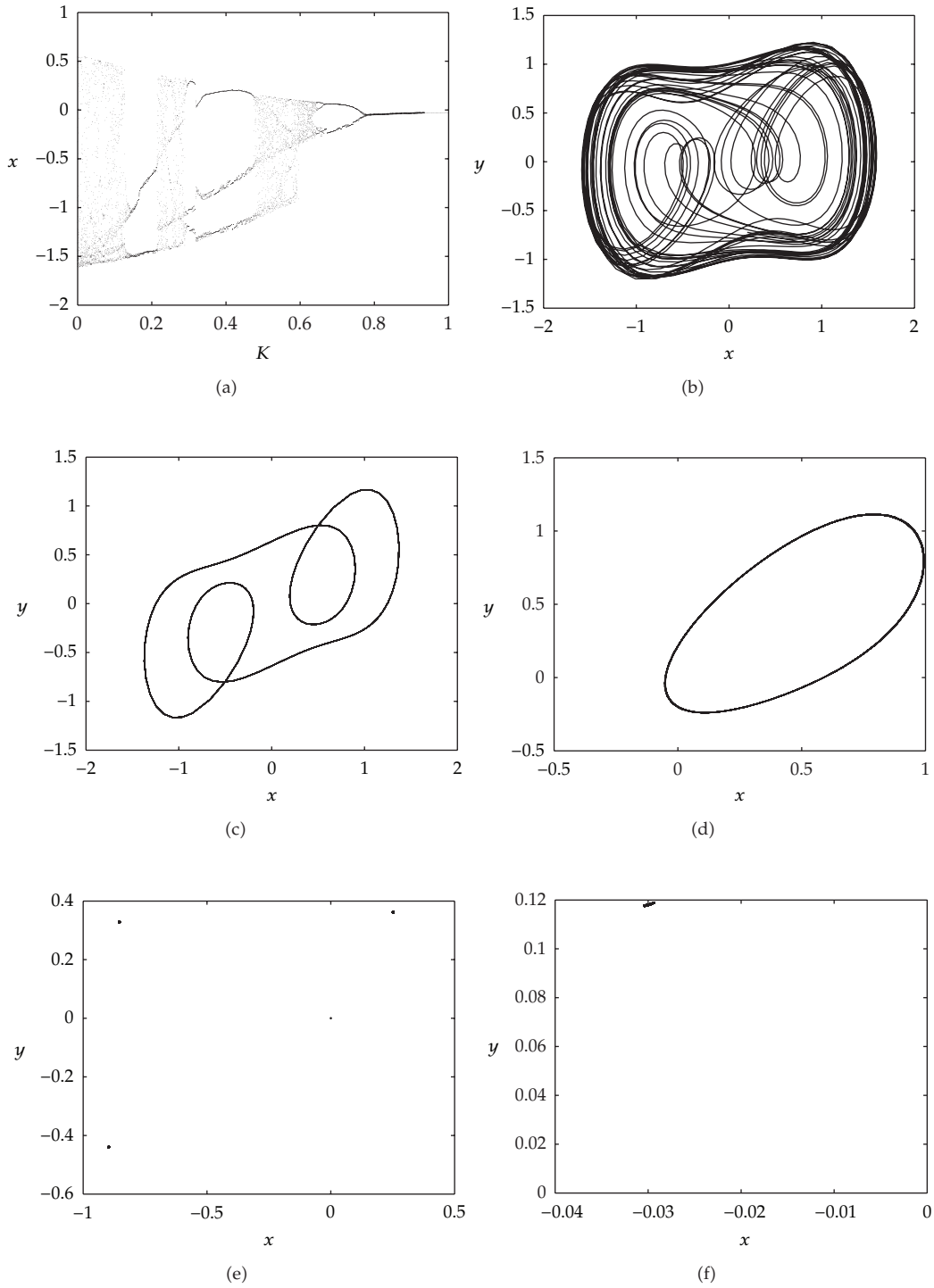

Figure 8: (a) Bifurcation diagram of the system (4.1) in $K \in (0,1)$. (b, c, and d) Phase portraits for three values of K in Figure 8(a). (e) Pioncaré map of the system (4.1) for $K = 0.4$. (f) Pioncaré map of the system (4.1) for $K = 0.8$.

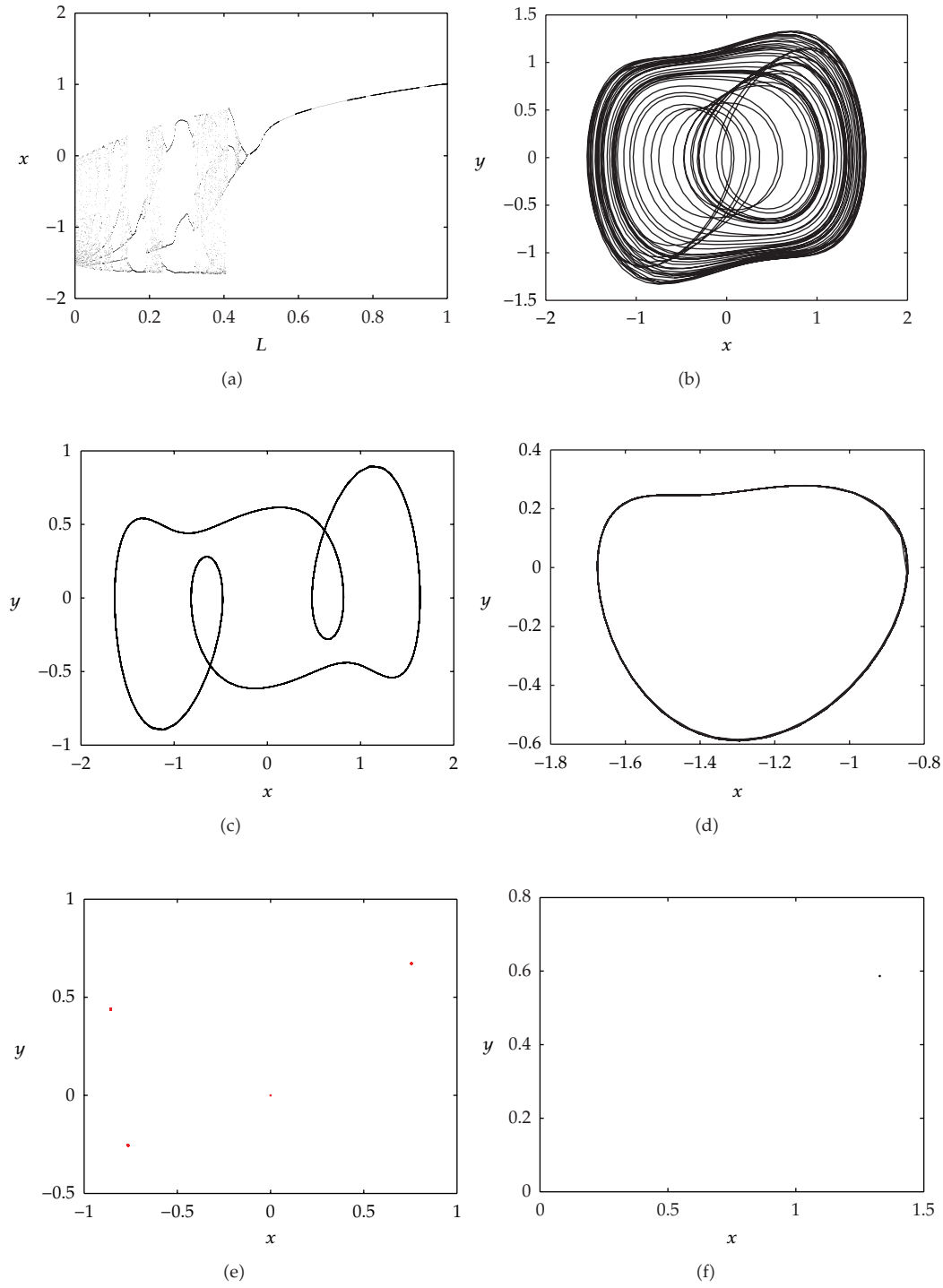

Figure 9: (a) Bifurcation diagram of the system (4.2) in $L \in (0,1)$. (b, c, and d) Phase portraits for three values of L in Figure 9(a). (e) Pioncaré map of the system (4.2) for $L = 0.3$. (f) Pioncaré map of the system (4.2) for $L = 0.8$.

4.2. Coupled Feedback Control

With the control signal $f(t) = L[x(t) - y(t)]$ coupled with the periodic signal $y(t)$ and the output $x(t)$ of the system (1.6), where L is the weight for the control signal to adjust the intensity, so we can get the the system(4.2)

$$\begin{aligned} \dot{x} &= y, \\ \dot{y} &= Fx - Dx^3 - \varepsilon\delta y - \varepsilon\delta_1 y^3 - \varepsilon\delta_2 y^2 x - \varepsilon\delta_3 x^2 y + \varepsilon r\cos\omega t + \varepsilon r_1 x - \varepsilon r_2 x^3 + L(x - y). \end{aligned} \tag{4.2}$$

The bifurcation diagram of the system (4.2) for $L \in (0, 1)$ is shown in Figure 9(a). We can see that the behavior of the system (4.2) remains chaotic as L increases from zero, period-2, 3, 5 windows within the chaotic regions, and the period-doubling bifurcations from period-2, 3, 5 orbits leading to chaos. When L arrives at and pass through a critical value $L \approx 0.41082$, the behavior changes from chaotic to periodic; namely, L suppresses chaos in the system (4.2). The phase portraits of different L ($L > 0$) in the system (4.2) are shown in Figures 9(b), 9(c), and 9(d): (b) $L = 0.001$ (chaos); (c) $L = 0.3$ (period-3 orbit); (d) $L = 0.8$ (period-1 orbit). The Pioncaré maps for $L = 0.3$ and $L = 0.8$ are shown in Figures 9(e) and 9(f). From Figure 9, we can also select the appropriate parameters to control chaos.

5. Conclusion

Applying Melnikov method, phase portraits, potential diagram, homoclinic bifurcation curve diagrams, bifurcation diagrams, and Pioncaré maps, the bifurcation and chaotic behavior of the system (1.3) and (1.6) are studied qualitatively and quantitatively. By numerical simulation, the impact of excitation amplitude r on the system (1.3) and (1.6) is analyzed respectively. Using two control methods on the system (1.3) and (1.6), respectively, the chaotic state is controlled effectively. Different control methods have different advantages and may be required to choose.

References

[1] G. Chen and T. Ueta, "Yet another chaotic attractor," *International Journal of Bifurcation and Chaos*, vol. 9, no. 7, pp. 1465–1466, 1999.

[2] L. O. Chua and G. N. Lin, "Canonical realization of Chua's circuit family," *IEEE Transactions on Circuits and Systems*, vol. 37, no. 7, pp. 885–902, 1990.

[3] G. Qi, G. Chen, S. Du, Z. Chen, and Z. Yuan, "Analysis of a new chaotic system," *Physica A*, vol. 352, no. 2–4, pp. 295–308, 2005.

[4] O. E. Rössler, "An equation for continuous chaos," *Physics Letters A*, vol. 57, no. 5, pp. 397–398, 1976.

[5] Z. Jing and R. Wang, "Complex dynamics in Duffing system with two external forcings," *Chaos, Solitons and Fractals*, vol. 23, no. 2, pp. 399–411, 2005.

[6] Z. Jing, Z. Yang, and T. Jiang, "Complex dynamics in Duffing-Van der Pol equation," *Chaos, Solitons and Fractals*, vol. 27, no. 3, pp. 722–747, 2006.

[7] Z. Jing, J. Huang, and J. Deng, "Complex dynamics in three-well Duffing system with two external forcings," *Chaos, Solitons and Fractals*, vol. 33, no. 3, pp. 795–812, 2007.

[8] J. Li et al., *Chaos and Menikov Method*, Chongqing University Press, China, 1989.

[9] S. Wang, *Differential Equation Model and Chaos*, China University of Science and Technology Press, China, 1999.

[10] J. Guckenheimer and P. Homel, *Nonlinear Oscillations, Dynamical System, and Bifurcation of Vectorfields*, Springer, Berlin, Germany, 1992.

[11] Z. Liu, *Perturbation Criterien for Chaos*, Shanghai Science and Technology Education Press, China, 1995.

[12] S. Wiggins, *Introduction to Applied Nonlinear Dynamical Systems and Chaos*, vol. 2 of *Texts in Applied Mathematics*, Springer, New York, NY, USA, 1990.